# Chapter 2

## Amide Functionalized Triazine Based 2D Porous Organic Polymer (MOP-Am2) to Promote Direct Deamination Reactions of Benzamides

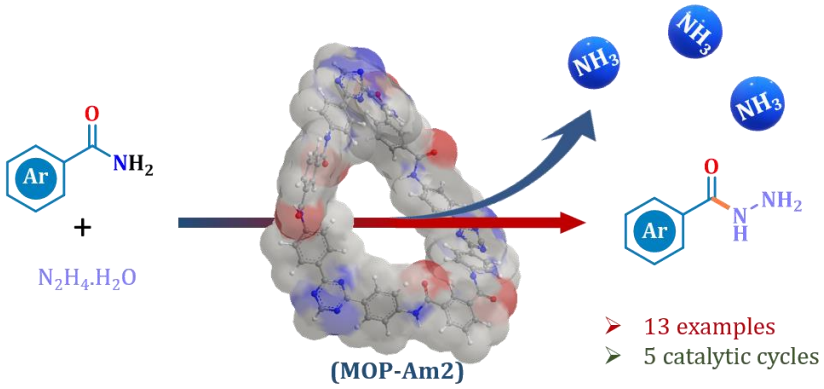

## 2.1 Introduction

Porous organic polymers (POPs) represent the periodicity of organic building units connected *via* strong covalent bond generating pores in its extended network. The topological construction of the organic building units determines the shape, size, functionality, and pore volume of POPs in the extended architecture [1]. A series of both 1D, 2D and 3D crystalline POPs have been reported since inception. In particular, 2D COFs have drawn significant interests because of the exceptional benefits of their extended in-plane-conjugation and topologically ordered columnar π-arrays [2,3]. It contains the polymer's crystallinity, porosity, and other properties including a smaller band gap and improved photocatalytic activity. The existence of π-cloud delocalization over the polymeric sheets causes the network to assume a planar shape. The high electron rich surface of the POPs prone to easy access to the targeted molecules *via* noncovalent interaction in a reaction media. This eventually activates the substrate molecules and accelerates or catalyse numbers of reactions. Additionally, the presence of delocalized π-clouds and covalent linkers provide the stability to the materials. The high thermal and chemical stability and insolubility in most of the common organic and inorganic solvents therefore makes POPs an excellent candidate for heterogeneous catalysis. Indeed, since Wang and coworkers demonstrated the Suzuki-Miyaura coupling process catalysed over Pd supported imine based POP in 2011, the applicability of such materials in the field of catalysis has skyrocketed in many folds [4-11].

Added metal catalyst on POPs may results traces of metal toxicity retaining in the desired product, thereby scaling out benign processes for organic transformation reactions. In search of benign and sustainable protocols, metal free POPs in catalysis are yet to be explored especially when it has the ability to enter the industrial scale of applications. It is evident from the literature that the imine linked POPs are predominantly explored in the realm of catalysis while compared among various other functionality such as ester, amide, imide and so on [12-16]. The free lone pair of electrons on the nitrogen atom in imine functional polymers provide interaction sites for changing the pace of the reaction. Unfortunately, the low wettability and stability of imine network in water undesirably hampers the diffusion in aqueous media and hence restricts the reusability. These undesirable features are bottleneck

that needs to be addressed especially for the modification in POPs with amide functionality for better practical applications [17].

The first known amide linked POP was illustrated in 2014, which was synthesized from *p*-phenylene diamine, trimesic acid and thionylchloride [18]. Later on in 2016, reports demonstrated the first two 2D amide linked POPs which were prepared *via* post-oxidation of imine based POPs. These prepared amide POPs showed improved chemical stability relative to their imine progenitors [19]. Highly polar amide functionality in POPs render easy Lewis acid-base interaction that allow such materials an excellent media to separate gases like $CO_2$ selectively over others [18,20]. The presence of basic functionality has also been exploited as a wonderful organocatalyst in performing organic transformation reaction [18,21-24]. Designing amide linked POPs with added multi-synergistic effects such as high porosity, photoactive framework, high wettability, and stability led to an unprecedented enhancement in the photocatalytic activity and recyclability [17]. Further investigation suggests that inclusion of heteroatom in the backbone of the POP network led to structural defects which enhances the catalytic activity by modulating multiple active sites [25]. Thereafter, only a few catalytic reactions have been imitated with metal free POP as heterogeneous catalyst.

Another advantage of amide linkage present in POPs is having H-bond donor-acceptor site that might behave as a facilitator in many organic transformation reactions *via* supramolecular interaction. This side of reaction with POPs is quite unknown and hence it opens up the window for catalytic activation of chemically inert molecules. One such example is the preparation of benzhydrazide derivatives *via* deamination of benzamide. This process of substituting $-NH_2$ is also known as transamidation reaction of benzamide.

Chemical structures having hydrazide moiety are a significant family of chemicals with several intriguing properties, including biological and pharmacological actions, as well as usefulness for analytical applications [26-32]. Many hydrazide derivatives have been prepared and found to exhibit a range of biological actions, including antibacterial anti-cancer and antiarrhythmic [33-37]. Furthermore, hydrazides may be easily transformed into hydrazones by treating them with aldehydes or ketones

[38]. Few biologically active known molecules having hydrazide moiety are exemplified below (Figure 2.1).

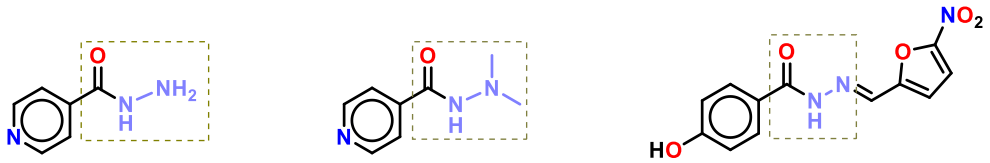


**Figure 2.1** Examples of biologically active hydrazide derivatives

However, a very few literatures are available for the synthesis of hydrazide moiety. The most popular method for making hydrazides is to combine hydrazines with anhydrides or acyl halides. The unstable substrates and harsh reaction conditions somewhat reduce the usability of these methods. Being easily available and stable precursor, benzamide has been an excellent choice for such conversation. However major disadvantages arise with $-NH_2$ as it is a bad leaving group. It is evident from the literature that the activation of the $-CONH_2$ using various metal complex such as $Fe(NO_3)_3 \cdot 9H_2O$ or hexagonal mesoporous silica with Brønsted acidic properties, etc. which eventually avoided the metal toxicity [39,40]. Metal free activation of benzamide approach is still keen to find. In 2014, chitosan has been demonstrated as an efficient metal free heterogeneous catalyst for the deamination of benzamide to hydrazide derivatives [41]. However, the reaction conditions or the reaction conversion were somehow compromised.

Few reported protocols for hydrazide derivatives synthesis *via* transamidation are highlighted below.

A. Fe(III) catalysed transamidation to benzhydrazide [39].

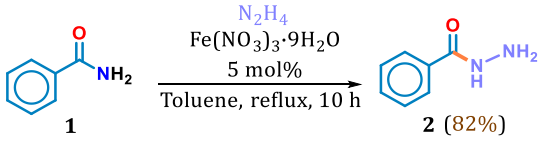


B. Brønsted acidic hexagonal mesoporous silica catalysed transamidation to benzhydrazide [40].

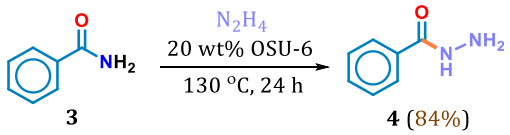

C. Chitosan catalysed transamidation to benzhydrazide [41].

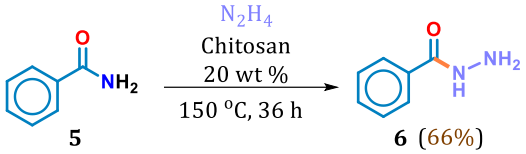


A couple of literatures are available for synthesizing hydrazides under different harsh condition. But protocols using a metal free recyclable catalyst is therefore a promising solution towards green and sustainable development. In this chapter, an amide functionalized triazine porous organic polymer, MOP-Am2 is designed and employed for the transamidation of benzamides under moderate condition.

*This work:*

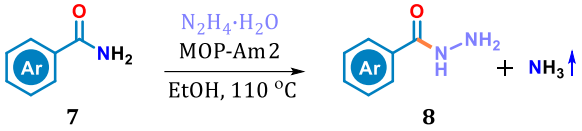


**Scheme 2.1** Transamidation or deamination of benzamide to benzhydrazide

The possible H-bonding from the amide functionality facilitated the activation of benzamide followed by reaction with hydrazine hydrate to give benzhydrazide derivatives which eventually eliminate $NH_3$ without using external metal source. The importance of the triazine moiety however discussed in the later chapters.

## 2.2 Results and Discussion

### 2.2.1 Synthesis of MOP-Am2-m

The monomeric unit MOP-Am2-m was synthesized following Scheme 2.2, which was used as a model reaction to proceed for the formation of extended amide functionalized solid. The chosen precursor of $C_3$ symmetric building unit TAPT (tris-(4-aminophenyl)-1,3,5-triazne) was first synthesized from trimerization reaction of 4-aminobenzonitrile in trifluoromethyl sulfonic acid [42]. 0.56 mmol of TAPT was dissolved in 15 mL of dry 1,4-dioxane and adding 1.68 mmol of triethylamine ($Et_3N$). To it 1.68 mmol of benzoyl chloride was slowly added. The resulted white precipitate of MOP-Am2-m was filtered and characterized with NMR spectroscopy. $^1$H NMR (400 MHz DMSO-$d_6$) δ (ppm): 10.64 (s, 3H), 8.78 (d, $J$ = 8.6 Hz, 6H), 8.12 (d, $J$ = 8.6 Hz, 6H), 8.03 (d, $J$ = 7.9 Hz, 6H), 7.65 – 7.55 (m, 9H).

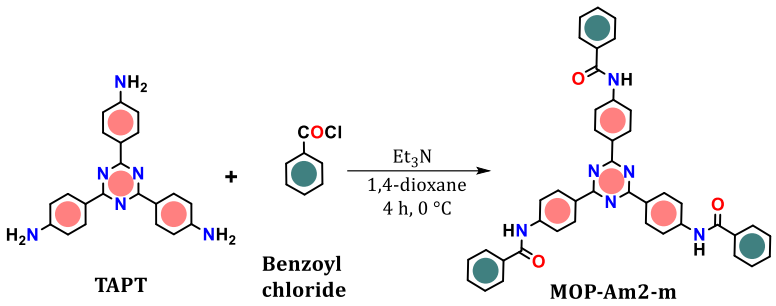


**Scheme 2.2** Synthesis of monomeric unit (MOP-Am2-m) of the amide functionalized porous organic polymer

### 2.2.2 Synthesis of MOP-Am2

Establishing the model reaction of the monomeric unit, we synthesized the extended network having amide functionality. In order to construct MOP-Am2 with well-defined hexagonal pores, a typical condensation reaction was performed with 0.14 mmol of $C_3$ symmetric TAPT and 0.14 mmol of $C_3$ symmetric 1,3,5-benzenetricarbonylchloride (BTCl) in 1,4-dioxane (Scheme 2.3). The pale-yellow precipitate obtained was filtered, washed several times with acetone to avoid unreacted side-products, and dried under vacuum at 100 ℃ for 24 h.

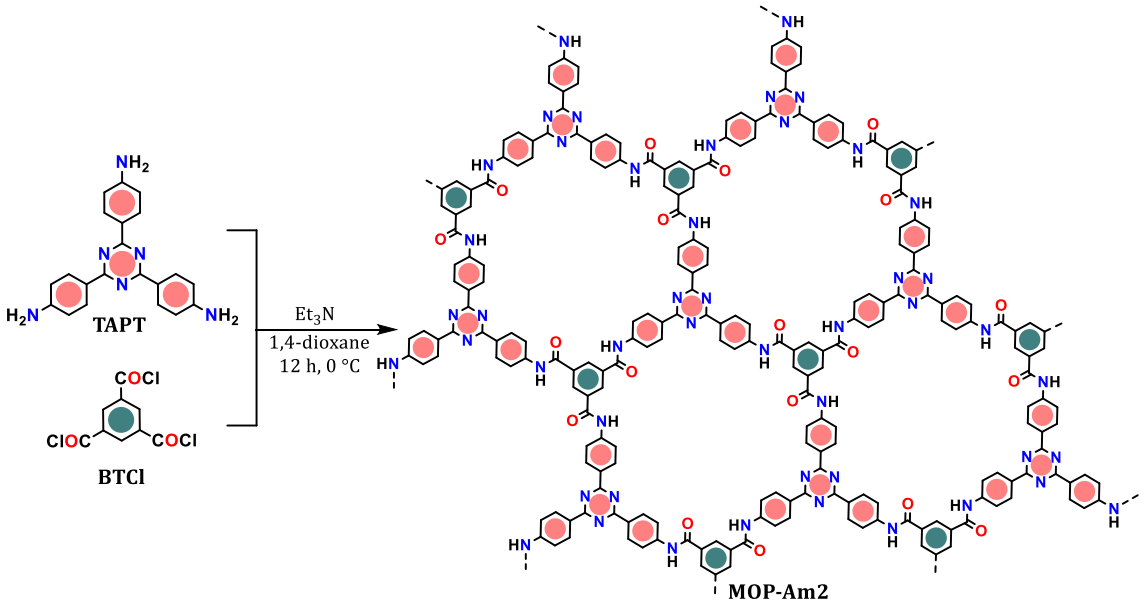


**Scheme 2.3** Synthesis of amide functionalized porous organic polymer, MOP-Am2

The structural integrity and functionality associated with MOP-Am2 were characterized with various spectroscopic, microscopic, thermal, diffraction and sorption analysis. The fine powder was preliminary investigated with Fourier

Transformed Infrared (FT-IR) spectroscopy analysis. As shown in Figure 2.2a the disappearance of stretching band for (O=C–Cl) at 1758 $cm^{-1}$ and reappearance at 1665 $cm^{-1}$ suggests the formation of amide (–HN–C=O) bond while the broad stretching band at 3363 $cm^{-1}$ signifies the existence of the amide (–HN–) in it. Due to the insolubility of MOP-Am2 in almost all the solvents, we could not process for the solution phase $^{1}H$ and $^{13}C$ NMR analyse. Besides the recorded solid state $^{13}C$ CP/MAS NMR spectroscopy reveals the significant signal at 163 ppm responsible for amide C=O of MOP-Am2 while the peaks at 152, 150, 141, 131, 120 and 118 ppm are assigned for the aromatic carbons (Figure 2.2b). In addition, the signals appearing at 170 ppm depicts the presence of intact triazine ring of MOP-Am2.

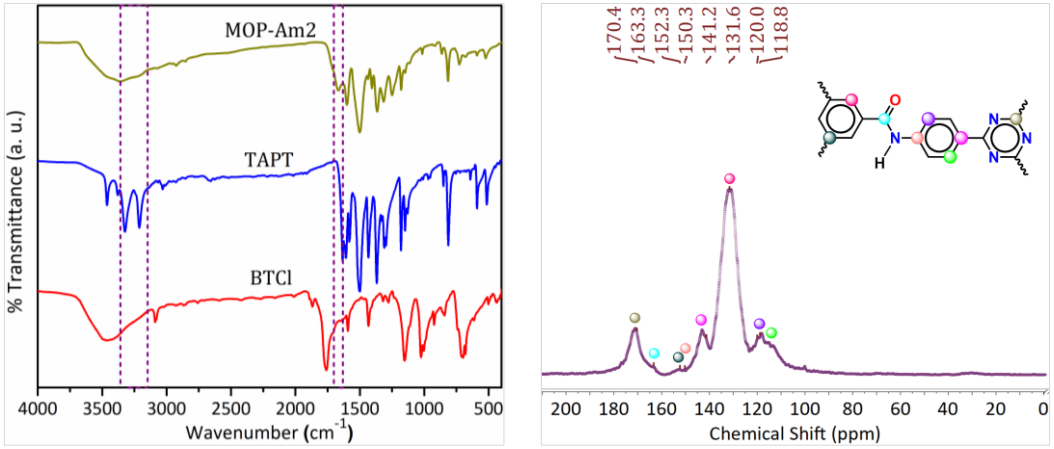


(a) (b)

**Figure 2.2** (a) Overlay FT-IR spectra analysis of MOP-Am2 with the corresponding reactants, TAPT and BTCl. (b) Solid state $^{13}C$ CP/MAS NMR spectrum of MOP-Am2

The crystalline behaviour of MOP-Am2 was validated with powder X-ray diffraction (PXRD) analysis. Several broad peak at 6.85°, 9.13°, 15.74°, 24.68° and 43.41° suggested a good agreement for reasonable crystallinity of MOP-Am2 (Figure 2.3a). The peak at 2θ=24.68° corresponds to an ordered layer structure with respect to the plane (100). The surface area and the pore dimension were examined using Brunauer-Emmett-Teller (BET) surface area analyser. The $N_2$ sorption isotherm measured at 77 K anticipated a type IV isotherm with calculated surface area of 51 $m^2g^{-1}$ (Figure 2.3b). Relatively low surface area was attributed due to the unordered skeleton structure and blockage of the channels entangled by outgrowth linkage arms during polymerization. Additionally, $N_2$ desorption isotherm has demonstrated a H1 type hysteresis that depicts the presence of cylindrical micropores [43]. Figure

2.3b (inset) has represented the pore size distribution plot with calculated narrow pore width distribution at 1.5 nm which also validates the nature of microporosity.

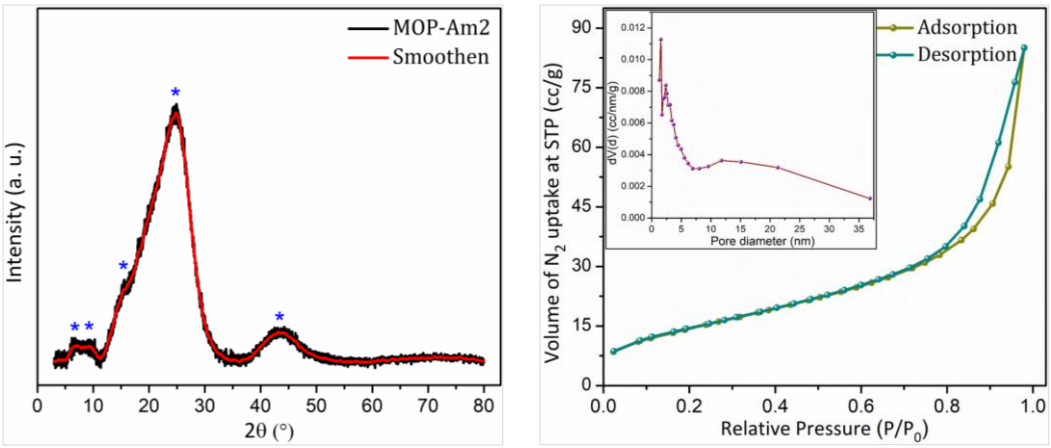


(a) (b)

**Figure 2.3** (a) powder X-ray diffraction pattern, and (d) BET sorption isotherm plot of $N_2$ at 77 K along with the pore size distribution plot (inset) of MOP-Am2

The morphological study and the elemental composition of MOP-Am2 was performed using electronic imaging analyses.

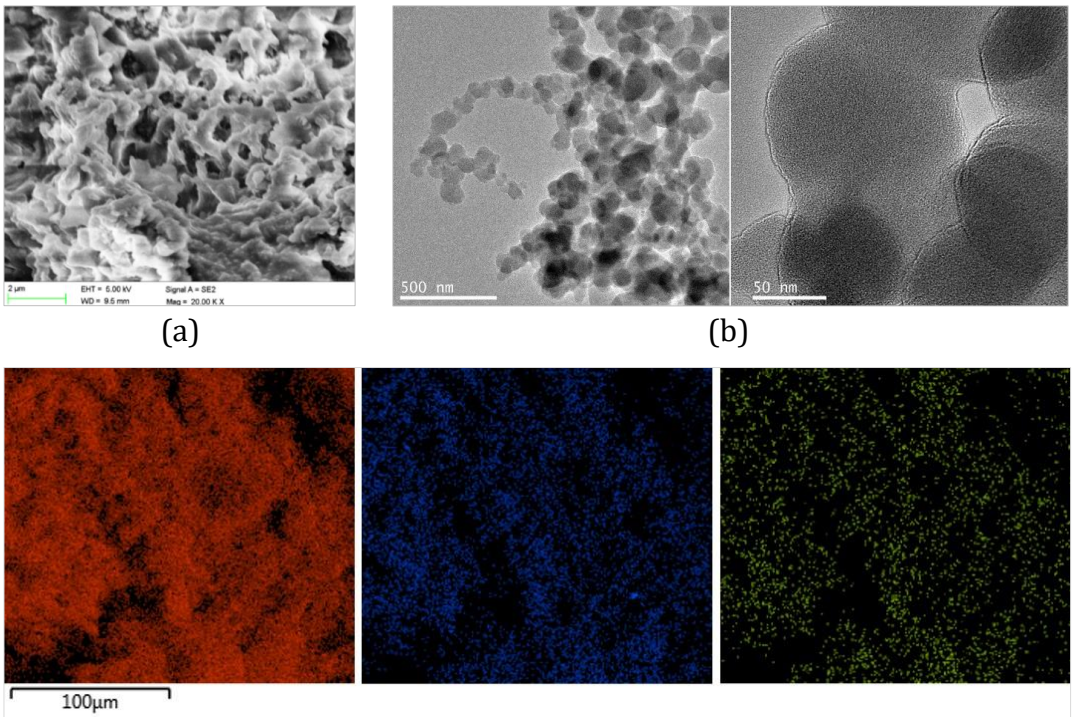


(a) (b)

(c)

**Figure 2.4** (a) FESEM image, (b) TEM image and (c) TEM-EDX elemental mapping of MOP-Am2. The uniform distribution the elements are designated with C (red), N (green) and O (blue)

The field emission scanning electron microscope (FESEM) analysis on MOP-Am2 depicted a spider-web-like rough morphology with clear visibility of pores (Figure 2.4a). While the transmission electron microscope (TEM) image represented a typical stacked 2D sheet or layered extended network structure (Figure 2.4b). This also validates the appearance of (100) plane that was observed during PXRD analysis. In addition, the elemental mapping based on TEM-energy dispersive X-ray spectrum (TEM-EDX) displayed a uniform distribution of C (red), N (green) and O (blue) in the MOP-Am2 (Figure 2.4c).

Since MOP-Am2 is polymeric in nature, thus the exact atomic percentage contents cannot be determined. However, the calculated atomic percentage content in the monomeric unit is estimated to be 76.9% (C), 15.3% (N) and 7.6% (O) whereas from the TEM-EDX spectrum, the atomic percentage content found are 73.5% (C), 14.7% (N) and 11.9% (Figure 2.5). These slight variations in atomic percentage content can be attributed from the presence of polar amide functionality having H-bonding ability towards atmospheric water. As a result, the percentage content of O increases while that of C and N decreases.

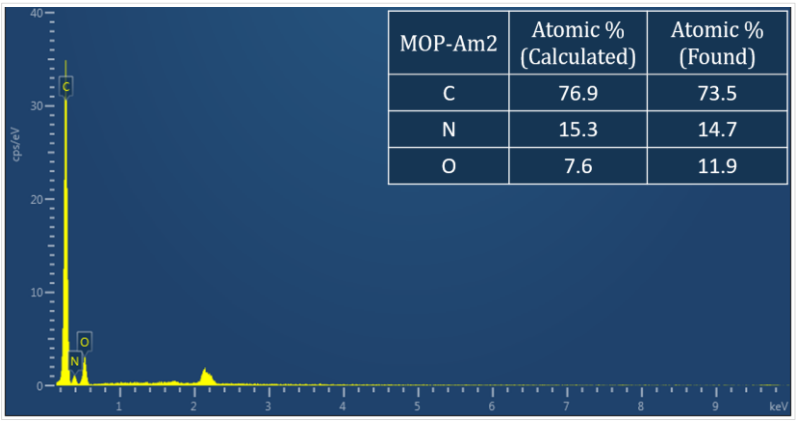


| MOP-Am2 | Atomic % (Calculated) | Atomic % (Found) |
|---|---|---|
| C | 76.9 | 73.5 |
| N | 15.3 | 14.7 |
| O | 7.6 | 11.9 |

**Figure 2.5** TEM-EDX spectrum with the atomic percentage content in MOP-Am2

### 2.2.3 Stability test for MOP-Am2

The thermal stability of MOP-Am2 was investigated using thermogravimetric analysis (TGA). It is evident from Figure 2.6a that the material is stable upto 480 °C in contrast to a trace amount of weight loss of 7.60% which might appear for the residual water molecule from the atmosphere. The affinity of MOP-Am2 towards atmospheric water was also reflected in the atomic percentage content in TEM-EDX

spectrum. Even though a small gradient in weight loss of 12.77% was observed at 352 °C, but most part of the MOP-Am2 decomposed at 480 °C.

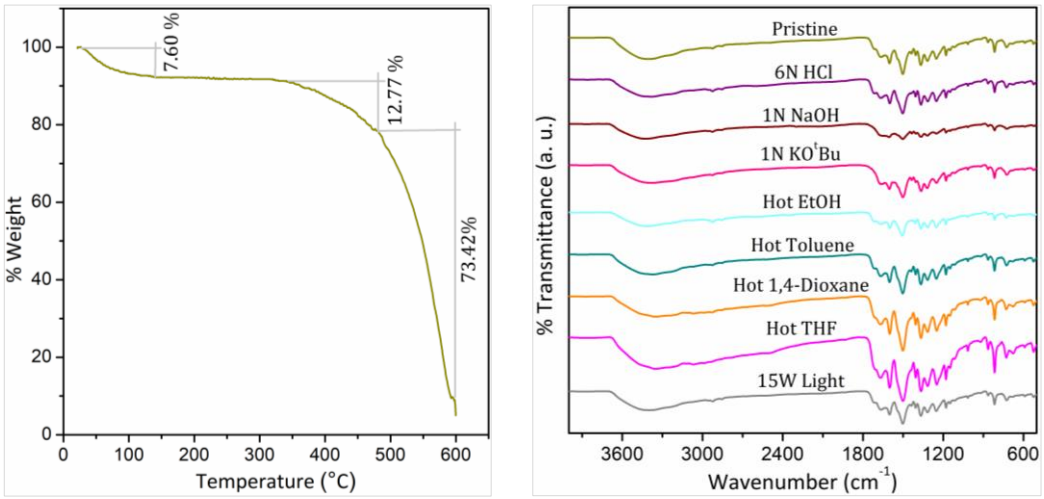


(a) (b)

**Figure 2.6** (a) TGA thermogram of MOP-Am2. (b) FT-IR spectra of MOP-Am2 at different chemical and physical environment.

The chemical stability of MOP-Am2 was examined by treating it with various organic, inorganic, acidic and basic solvents in both room temperature and hot condition for 2 days. As determined by FT-IR analysis in Figure 2.6b, the recovered dry MOP-Am2 affirmed intact structural integrity even after irradiating it with 15W LED light. The high stability towards harsh chemicals and physical parameter are added features to the electron rich surface of MOP-Am2 that renders it a potential candidate in heterogeneous catalysis.

### 2.2.4 Catalytic deamination of benzamide

The amide moiety in MOP-Am2 is a well-known synthon both as H-bond donor and acceptor. Deciphering the feasibility and important aspects of amide functionality in the extended solids as heterogeneous catalyst, deamination reaction of benzamides has been chosen as benchmark reaction during benzhydrazides synthesis (Scheme 2.1).

The components responsible for the transformation *viz.* solvents, sacrificial agents and catalyst necessities were resolved and presented accordingly in Table 2.1. The reaction was optimized by taking benzamide as the initial substrate.

**Table 2.1** Reaction optimization for deamination or transamidation of benzamide to benzhydrazide.[a]

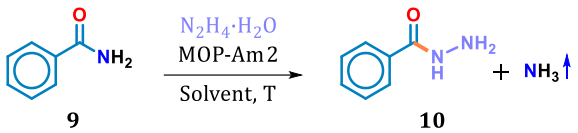


9 10

| Entry | MOP-Am2 (wt %) | Solvent (mL) | T (°C) | Time (h) | **10** % Yield[b] |
|---|---|---|---|---|---|
| 1 | 3 | EtOH | 90 | 7 | 46 |
| 2 | 3 | EtOH | 100 | 7 | 53 |
| 3 | 3 | EtOH | 110 | 7 | 65 |
| 4 | 3 | EtOH | 120 | 7 | 66 |
| 5 | 3 | EtOH | 110 | 6 | 60 |
| 6 | 3 | EtOH | 110 | 8 | 72 |
| 7 | 3 | EtOH | 110 | 9 | 72 |
| 8 | - | EtOH | 110 | 8 | 23 |
| 9 | 3 | EtOH | 110 | 8 | 65 |
| 10 | 5 | EtOH | 110 | 8 | 77 |
| 11 | 8 | EtOH | 110 | 8 | 84 |
| 12 | 10 | EtOH | 110 | 8 | 85 |
| 13 | 12 | EtOH | 110 | 8 | 85 |
| 14 | 8 | Toluene, $CH_3CN$, $H_2O$ | 110 | 8 | NR |

[a]Reaction conditions: **9** (0.5 mmol), $N_2H_4{\cdot}H_2O$ (0.75 mmol), MOP-Am2 (8 wt% of benzamide), EtOH (1 mL), T (110 °C), time (8 h). [b]Characterized with LCMS. NR: No reaction.

Initially the reaction was tested with 0.5 mmol of benzamide with gradually increasing the concentration of $N_2H_4{\cdot}H_2O$ in presence of 3 wt% MOP-Am2 and 1mL of ethanol at 140 °C. Reaction progress was monitored using TLC and at the end of 7 h of reaction time, it was found that 0.75 mmol of $N_2H_4{\cdot}H_2O$ against 0.5 mmol of benzamide resulted the maximum conversion. On optimization with a range of temperature taking other conditions identical, increased productivity was observed at 110 °C (Table 2.1, entry 1-4). Upon increasing the reaction time to 8 h, the conversion was enhanced further (Table 2.1, entry 5-7).

The reaction was also tested without the catalyst. Interestingly the result was affirmative. However, the reaction comparatively showed low conversion (Table 2.1, entry 8). This clearly indicates the significance of MOP-Am2 as heterogeneous support catalyst for better reaction conversion. Optimization of the catalyst loading necessary for the maximum conversion was attained at 8 wt% with respect to benzamide (Table 2.1, entry 9-13). To check the solvent effects, other solvents such as Toluene, $CH_3CN$, $H_2O$ were also examined (Table 2.1, entry 14). Unfortunately, the reaction did not proceed.

### 2.2.5 Substrate scope study

With the optimized reaction conditions, substrate scope study is performed with diverse amides to confirm the affordability of the protocol and are summarized in Table 2.2.

**Table 2.2** Substrate scope study for deamination of benzamide derivatives to their corresponding hydrazides.[a]

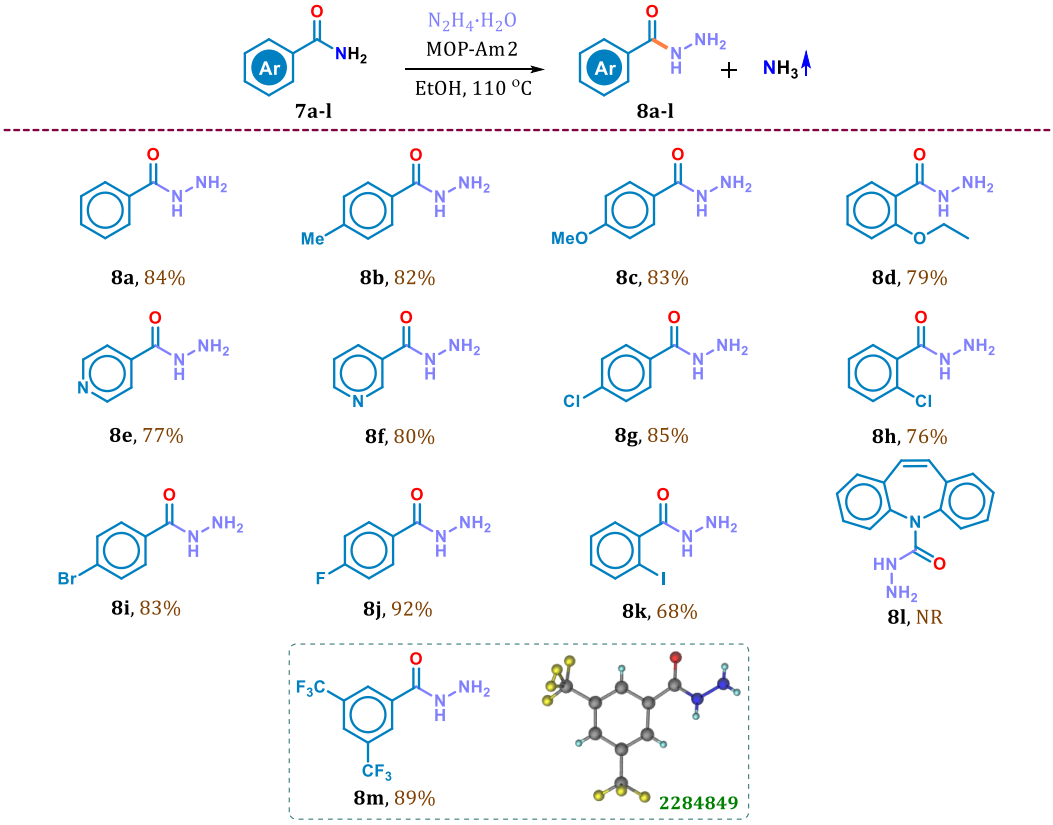


[a]Reaction conditions: **7a-l** (0.5 mmol), MOP-Am2 (8 wt% w. r. t. **7**), $N_2H_4{\cdot}H_2O$ (0.75 mmol), EtOH (1 mL), T (110 °C), time (8 h). [b]Characterized with LCMS. NR= No reaction, CCDC No. (Green colour).

Approximately thirteen substrate molecules have been studied with different substituents and the catalyst performed well with reaction conversion upto 92%. Electron donating substituents on *para* position did not hamper the yield much, **8a-8c**. On the other hand, *o*-ethoxy substitution possessed relatively lower conversion yield of 79%, **8d**. The protocol even worked on heterocyclic amide **8e** & **8f** and established synthesis of pharmaceutically active molecule isoniazid (used to treat tuberculosis), **8e**. Positional isomers of chlorobenzamides showed significant difference in yield, **8g** & **8h**. Again *p*-bromobenzamide resulted less conversion when compared to *p*-fluorobenzamide, **8i** & **8j**. Even *p*-fluoro- substitution showed the highest reaction conversion of 92% among the halogenated benzamide. While the *o*-iodobenzamide possessed the lowest conversion of 68%, **8k** which might because of the steric factor as well as its bulkiness and low electronegativity that makes the $-CONH_2$ less electropositive. No reaction was observed when carbamazepine was tested for transamidation. Instead, the amide moiety detached from the substrate molecule. While, di-substituted highly electron withdrawing substituents ($-CF_3$) at *meta* position showed excellent conversion of 89%, **8m**. Crystal structure of **8m** was cultivated in chloroform and analysed with single crystal X-diffraction analysis.

### 2.2.6 Mechanism

The mechanism involved during the deamination of benzamide was believed to proceed *via* weak H-bonding. Literature witnessed the use of H-bonding in benzamide activation [43,44]. Principles of crystal engineering imply two binding sites for benzamide on MOP-Am2 *via* N–H···O interaction; either Path A or Path B (Figure 2.7a). To find out the energetically more favourable path, computational study has been performed. With the limited competence it was difficult to carry a computational study on the catalytic behaviour of polymeric MOP-Am2. Since the monomeric unit, MOP-Am2-m is essentially an active catalyst for the reactions studied, we reflected the same in place of MOP-Am2 structure for calculation. The structural optimization and various active binding sites for the interaction with benzamide were carried out with B3LYP/6-31G(d) level of theory. Prior to both the active sites, Path A is energetically more favourable by 2.74 kcal/mol over Path B. The N–H···O bond distance between the amide and the catalyst is calculated to be 1.834 Å that induces δ+ centre on carbonyl carbon *via* H-bonding (Figure 2.7b).

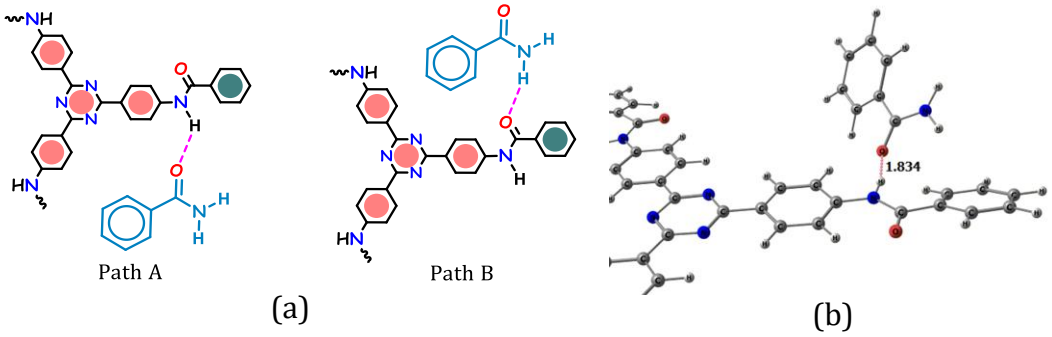


**Figure 2.7** (a) Possible binding site for amide substrate on MOP-Am2-m. (b) Optimized geometry of N–H···O interaction from MOP-Am2-m to the benzamide. Bond length is in Å

Visual illustration of the plausible mechanism involved during the synthesis of hydrazide is depicted in Figure 2.8. The incoming nucleophile, $N_2H_4{\cdot}H_2O$ thus attacked the carbonyl centre *via* activated amide intermediate. Subsequent rearrangement to step III, proton transfer took place while moving to step IV converting the amide $-NH_2$ as ammonium ion. Finally, the delocalization served as the driving force thereby eliminating $NH_3$ to yield the desired transamidation product along with regenerating the catalyst MOP-Am2 for another cycle.

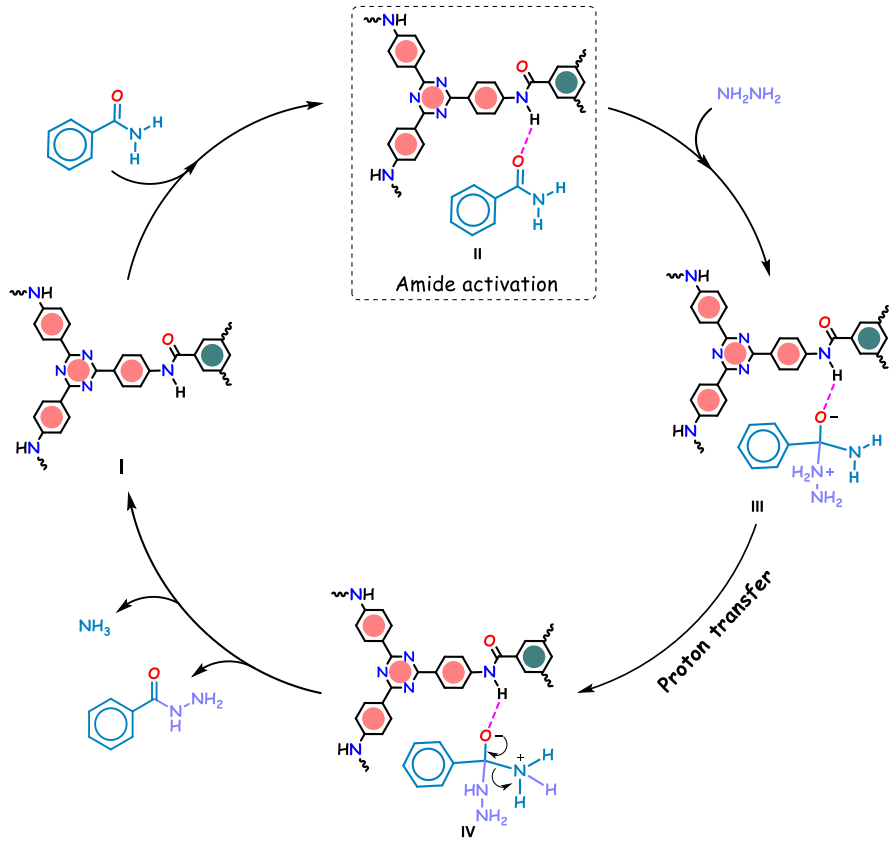


**Figure 2.8** Plausible mechanism of trasamidation of benzamide over MOP-Am2

### 2.2.7 Catalytic cycle and reusability

The major concerns about any catalyst in any domain of chemical conversion reactions are recyclability and efficiency. To check the heterogeneity, we have chosen the transamidation of benzamide to its corresponding hydrazide at the optimized reaction conditions. The reusability test indicated the high efficiency of the catalyst MOP-Am2 as a promoter upto the 5$^{th}$ cycles (Figure 2.9a).

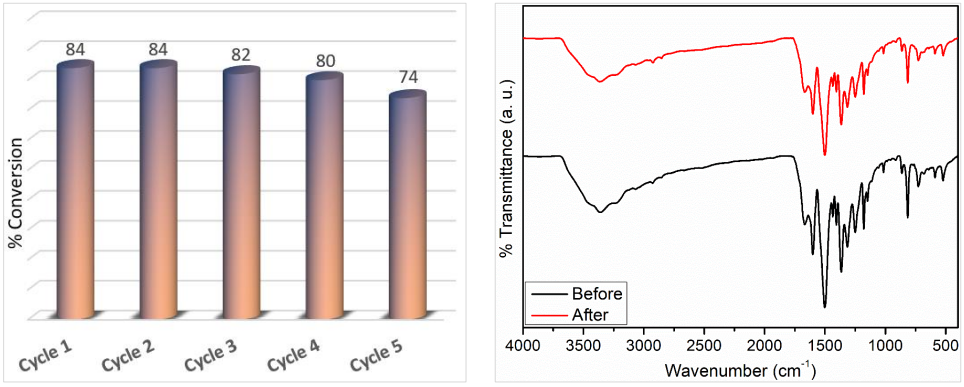


(a) (b)

**Figure 2.9** (a) Catalyst reusability test up to 5$^{th}$ cycle. (b) FT-IR spectra of MOP-Am2 before and after 5$^{th}$ cycle of the reaction

Another concern regarding the protocol is that both substrates and the catalyst contained amide functionality. Therefore, there is a high probability of the catalyst being reacted by $N_2H_4 \cdot H_2O$ along with the substrate molecule. $N_2H_4 \cdot H_2O$ is also well-known as a reducing agent for hydrogenation. Hence it is mandatory to confirm the selectivity of the reaction that occurred only at the substrate molecules keeping the catalyst unreacted. To check the structural integrity remained uneffaced, the catalyst was recovered *via* filtration after each cycle, dried and characterized with FT-IR analysis. Figure 2.9b depicted no variation in FT-IR spectra when compared with before and after 5$^{th}$ cycle of the reaction and thus affirmed the intact structural integrity of MOP-Am2.

### 2.3 Summary

This chapter has covered the strategic design and synthesis of amide functionalized triazine based 2D porous organic polymer (MOP-Am2) from [$C_3$+$C_3$] symmetric condensation of TAPT and BTCl. The structural integrity of the obtained the MOP-

Am2 were determined with various thermal, microscopic, diffraction, sorption and spectroscopic techniques.

The presence of amide functionality in POPs conveyed a vital role as heterogeneous surface in catalytic Knoevenagel condensation, selective $CO_2$ capture, gold recovery, etc. Here the amide functionality in MOP-Am2 has been exploited as heterogeneous activating agent in the deamination of benzamide *via* weak H-bonding. The polar amide moiety is a well-known supramolecular synthon that may function either as an H-bond donor or an acceptor. DFT study on the reaction mechanism has validated the existence of weak interaction of benzamide through amide scaffold of the catalyst. In addition, MOP-Am2 behaved as an effective facilitator for converting $-NH_2$ to a good leaving group liberating as $NH_3$ avoiding any external activating agent. Diverse substrate scope study has been carried out with excellent productivity up to five catalytic cycles while retaining the structural integrity of the catalyst for subsequent applications.

## 2.4 Experimental Section

### 2.4.1 Materials and methods

All the chemicals employed were purchased from commercial sources (Sigma Aldrich, Alfa Aesar and Merck) and were used as such without further purification until otherwise mentioned. FT-IR spectra were recorded in the range 400-4000 $cm^{-1}$ by preparing the sample pellets in KBr using Perkin Elmer spectrophotometer.

The powder X-ray diffraction (PXRD) was recorded in D8 ADVANCE X-ray using monochromated Cu Kα (λ = 1.542 Å) radiation made by Bruker. Thermogravimetric analyses (TGA) were performed on a Shimadzu 60 thermal analyzer at a heating rate of 10 °C $min^{-1}$ under continuous $N_2$ flow. $N_2$ adsorption-desorption isotherm were recorded in Quantachrome (Version 3.0) surface area analyzer. The liquid nitrogen used in the measurement was of ultra-high purity (99.999% pure) and the refrigerated bath of liquid nitrogen (77 K) further controls the temperature during the process.

Field emission scanning electron microscope (FESEM) images were recorded in Gemini 500 FESEM (software: SmartSEm User Interface). Transmission electron

microscope (TEM) images and TEM-EDX spectrum were recorded in JEOL JEM 2100 at an accelerating voltage of 200 kV to examine the surface and bulk morphology.

Solid state $^{13}C$ cross polarizing magic angle spinning ($^{13}C$ CP/MAS) NMR data was recorded in Jeol 400 MHz spectrometer employing 4 nm MAS probe with spin rate of 5000 Hz. The progress of the reactions was monitored by TLC using TLC silica gel F254 250 μm precoated-plates from Merck and the product formation was confirmed by NMR spectrometer (Bruker AVANCE NEO NMR SPECT. 400 MHz), and LCMS was recorded on Agilent 6125 SQ system.

### 2.4.2 Synthesis of tris-(4-aminophenyl)-1,3,5-triazine (TAPT)

TAPT was synthesized following the reported procedure. Triflic acid (2 mL) was taken in a 10 mL round bottom flask and to it 4-aminobenzonitrile (0.720 g) was added keeping the temperature below -5 °C and the reaction was run for 6 hours under $N_2$ environment. To the reaction mixture, 10 mL distilled water was added followed by addition of 2M NaOH dropwise until the clear red solution gave a bright yellow precipitate at pH=7. The desired precipitate of TAPT was then washed with distilled water, dried and characterized it with NMR analysis. $^1H$ NMR (400 MHz, DMSO-$d_6$) δ (ppm): 8.31 (d, *J* = 8 Hz, 6H), 6.65 (d, *J* = 8 Hz, 6H), 5.89 (s, 6H). $^{13}C\{^1H\}$ (101 MHz, DMSO-$d_6$) δ (ppm): 170.1, 153.5, 130.7, 123.4, 113.6.

### 2.4.3 Synthesis of monomeric MOP-Am2-m

MOP-Am2-m was synthesized using reported procedure. Dissolved 200 mg (0.56 mmol) of TAPT in 15 mL of dry 1,4-dioxane and adding 1 mL of triethylamine ($Et_3N$). To it 170 μL (1.68 mmol) of benzoyl chloride was slowly added in nitrogenous environment and left with continuous stirring for 4 h. The desired precipitate of MOP-Am2-m was then filtered, washed with 1,4-dioxane, dried in desiccator for 24 h and characterized with NMR analysis.

### 2.4.4 Synthesis of MOP-Am2

The MOP-Am2 was synthesized from TAPT and 1,3,5-benzenetricarbonyl trichloride (BTCl). Taking a 250 mL two neck round bottom flask, an amount of 354 mg (1 mmol) of TAPT was dissolved in 25 mL of dry 1,4-dioxane and kept in an ice cold water bath and additionally 3 mmol of triethylamine ($Et_3N$) was added in it. A solution of 265

mg (1 mmol) BTCl in dry 1,4-dioxane (10 mL) was slowly added over a period of 2 h in nitrogenous environment and left with continuous stirring for 12 h. Special care was taken while performing the reaction as it liberates corrosive HCl gas during condensation. The liberated HCl gas was trapped with $Et_3N$ which was then easily removed during filtration. The desired precipitate of MOP-Am2 was then filtered and washed with acetone. The solubility of all other unreacted particle and undesired product except the desired one allow us to get a pure expected porous material. The material was then dried in desiccator for 24 h to remove the surface captured solvent molecules and then characterized.

### 2.4.5 Computational details

Gaussian 09 software package was used to perform Density Functional Theory (DFT) calculations to obtain the geometry optimizations, ground state energies and vibrational frequencies of the species in interest [45]. A popular and dependable Becke-3-parameter-Lee-Yang-Parr B3LYP functional along with 6-31G(d) basis set is chosen for the geometry optimizations.

### 2.4.6 Transamidation of aromatic amides to corresponding hydrazides

A schlenk tube was filled with 0.5 mmol of aromatic amide derivatives in 1 mL of ethanol. To it 0.75 mmol of hydrazine hydrate ($N_2H_4 \cdot H_2O$) and 8 wt % of MOP-Am2 were added with respect to the amide derivatives. The reaction mixture was stirred at 110 °C for 8 h. The reaction was monitored using TLC in 40% ethyl acetate:*n*-hexane as eluent. The product was purified using column chromatography with Silica Gel (60-120 mesh) and 10% ethyl acetate:*n*-hexane as eluent. The product was then identified with LCMS analysis.

### 2.4.7 Single crystal X-ray diffraction

Colourless plate-like crystals of **8m** were obtained from $CHCl_3$. Single crystal data was collected on a Bruker SMART APEX-II CCD diffractometer using Mo Kα (λ =0.71073 Å) radiation. Bruker-SAINT software was employed for reducing the data and SADABS for correcting intensity absorption. Structures were solved and refined using SHELXL with anisotropic displacement parameters for non-H atoms. C–H

atoms were fixed geometrically using the HFIX command in SHELX-TL. PLATON was used for correction in error for missing symmetry.

## 2.5 Bibliography

[1] Kandambeth, S., Dey, K., and Banerjee, R. Covalent organic frameworks: chemistry beyond the structure. *Journal of the American Chemical Society*, 141(5):1807-1822, 2018.

[2] Chen, X., Addicoat, M., Irle, S., Nagai, A., and Jiang, D. Control of crystallinity and porosity of covalent organic frameworks by managing interlayer interactions based on self-complementary π-electronic force. *Journal of the American Chemical Society*, 135(2):546-549, 2013.

[3] Ma, H., Liu, B., Li, B., Zhang, L., Li, Y. G., Tan, H. Q., Zang, H. Y., and Zhu, G. Cationic covalent organic frameworks: a simple platform of anionic exchange for porosity tuning and proton conduction. *Journal of the American Chemical Society*, 138(18):5897-5903, 2016.

[4] Ding, S. Y., Gao, J., Wang, Q., Zhang, Y., Song, W. G., Su, C. Y., and Wang, W. Construction of covalent organic framework for catalysis: Pd/COF-LZU1 in Suzuki–Miyaura coupling reaction. *Journal of the American Chemical Society*, 133(49):19816-19822, 2011.

[5] Ding, S. Y. and Wang, W. Covalent organic frameworks (COFs): from design to applications. *Chemical Society Reviews*, 42(2):548-568, 2013.

[6] Kaur, P., Hupp, J. T., and Nguyen, S. T. Porous organic polymers in catalysis: opportunities and challenges. *ACS Catalysis*, 1(7):819-835, 2011.

[7] Bhadra, M., Sasmal, H. S., Basu, A., Midya, S. P., Kandambeth, S., Pachfule, P., Balaraman, E., and Banerjee, R. Predesigned metal-anchored building block for in situ generation of Pd nanoparticles in porous covalent organic framework: application in heterogeneous tandem catalysis. *ACS Applied Materials & Interfaces*, 9(15):13785-13792, 2017.

[8] Bhadra, M., Kandambeth, S., Sahoo, M. K., Addicoat, M., Balaraman, E., and Banerjee, R. Triazine functionalized porous covalent organic framework for photo-organocatalytic E–Z isomerization of olefins. *Journal of the American Chemical Society*, 141(15):6152-6156, 2019.

[9] Zhang, T., Xing, G., Chen, W., and Chen, L. Porous organic polymers: a promising platform for efficient photocatalysis. *Materials Chemistry Frontiers*, 4(2):332-353, 2020.

[10] Sasmal, H. S., Bag, S., Chandra, B., Majumder, P., Kuiry, H., Karak, S., Sen Gupta, S., and Banerjee, R. Heterogeneous C–H functionalization in water *via* porous covalent organic framework nanofilms: a case of catalytic sphere transmutation. *Journal of the American Chemical Society*, 143(22):8426-8436, 2021.

[11] Kumar, P., Das, A., and Maji, B. Phosphorus containing porous organic polymers: synthetic techniques and applications in organic synthesis and catalysis. *Organic & Biomolecular Chemistry*, 19(19):4174-4192, 2021.

[12] Jagadesan, P., Eder, G., and McGrier, P. L. The excited-state intramolecular proton transfer properties of three imine-linked two-dimensional porous organic polymers. *Journal of Materials Chemistry C*, 5(23):5676-5679, 2017.

[13] Yang, J., Xu, M., Wang, J., Jin, S. and Tan, B. A facile approach to prepare multiple heteroatom-doped carbon materials from imine-linked porous organic polymers. *Scientific Reports*, 8(1):4200-4210, 2018.

[14] Samui, A., Kesharwani, N., Haldar, C., and Sahu, S. K. Fabrication of nanoscale covalent porous organic polymer: An efficacious catalyst for Knoevenagel condensation. *Microporous and Mesoporous Materials*, 299:110112, 2020.

[15] Li, T., Atish, C., Silambarasan, K., Liu, X., and O'Mullane, A. P. Development of an interfacial osmosis diffusion method to prepare imine-based covalent organic polymer electrocatalysts for the oxygen evolution reaction. *Electrochimica Acta*, 362:137212, 2020.

[16] Chakrabortty, P., Biswas, S., Das, A., Dolai, M., and Islam, S. M. Diformylphloroglucinol derived imine based covalent organic frameworks (PHTA) as efficient organocatalyst for conversion of isocyanates to urea derivatives. *Molecular Catalysis*, 522:112213, 2022.

[17] Ma, S., Li, Z., Jia, J., Zhang, Z., Xia, H., Li, H., Chen, X., Xu, Y., and Liu, X. Amide-linked covalent organic frameworks as efficient heterogeneous photocatalysts in water. *Chinese Journal of Catalysis*, 42(11):2010-2019, 2021.

[18] Suresh, V. M., Bonakala, S., Atreya, H. S., Balasubramanian, S., and Maji, T. K. Amide functionalized microporous organic polymer (Am-MOP) for selective

$CO_2$ sorption and catalysis. *ACS Applied Materials & Interfaces*, 6(7):4630-4637, 2014.

[19] Waller, P. J., Lyle, S. J., Osborn Popp, T. M., Diercks, C. S., Reimer, J. A., and Yaghi, O. M. Chemical conversion of linkages in covalent organic frameworks. *Journal of the American Chemical Society*, 138(48):15519-15522, 2016.

[20] Manoranjan, N., Kim, J., and Woo, S. I. Amide linked conjugated porous polymers for effective $CO_2$ capture and separation. *Journal of $CO_2$ Utilization*, 16:486-491, 2016.

[21] Kundu, S. K. and Bhaumik, A. A triazine-based porous organic polymer: a novel heterogeneous basic organocatalyst for facile one-pot synthesis of 2-amino-4 H-chromenes. *RSC Advances*, *5*(41):32730-32739, 2015.

[22] Khatioda, R., Talukdar, D., Saikia, B., Bania, K. K., and Sarma, B. Constructing two dimensional amide porous polymer to promote selective oxidation reactions. *Catalysis Science & Technology*, 7(14):3143-3150, 2017.

[23] Li, Y., Chen, W., Gao, R., Zhao, Z., Zhang, T., Xing, G., and Chen, L. 2D covalent organic frameworks with built-in amide active sites for efficient heterogeneous catalysis. *Chemical Communications*, 55(96):14538-14541, 2019.

[24] Sarma, P., Sarmah, K. K., Kakoti, D., Mahanta, S. P., Adassooriya, N. M., Nandi, G., Das, P. J., Bučar, D. K., and Thakuria, R. A readily accessible porous organic polymer facilitates high-yielding Knoevenagel condensation at room temperature both in water and under solvent-free mechanochemical conditions. *Catalysis Communications*, 154:106304, 2021.

[25] Lin, C. Y., Zhang, D., Zhao, Z., and Xia, Z. Covalent organic framework electrocatalysts for clean energy conversion. *Advanced Materials*, 30(5):1703646, 2018.

[26] Shamsabadi, A. and Chudasama, V. An overview of the synthesis of acyl hydrazides from aldehydes and reactions of the products thereof. *Organic & Biomolecular Chemistry*, 15(1):17-33, 2017.

[27] Wei, X. Z., Fu, Y. L., Xue, M. J., and Song, Q. H. Synthesis of oxadiazolones with hydrazides: the mechanism and the sensing application as sensitive, rapid, and visual fluorescent sensors for phosgene. *Organic Letters*, 21(23):9497-9501, 2019.

[28] Spiliopoulou, N., Constantinou, C. T., Triandafillidi, I., and Kokotos, C. G. Synthetic approaches to acyl hydrazides and their use as synthons in organic synthesis. *Synthesis*, 52(21):3219-3230, 2020.

[29] Wang, H., Jung, H., Song, F., Zhu, S., Bai, Z., Chen, D., He, G., Chang, S., and Chen, G. Nitrene-mediated intermolecular N–N coupling for efficient synthesis of hydrazides. *Nature Chemistry*, 13(4):378-385, 2021.

[30] Joly, N., Bettoni, L., Gaillard, S., Poater, A., and Renaud, J. L. Phosphine-free ruthenium complex-catalyzed synthesis of mono- or dialkylated acyl hydrazides *via* the borrowing hydrogen strategy. *The Journal of Organic Chemistry*, 86(9):6813-6825, 2021.

[31] Bettoni, L., Joly, N., Lohier, J. F., Gaillard, S., Poater, A., and Renaud, J. L. Ruthenium-catalyzed three-component alkylation: a tandem approach to the synthesis of nonsymmetric *N,N*-dialkyl acyl hydrazides with alcohols. *Advanced Synthesis & Catalysis*, 363(16):4009-4017, 2021.

[32] Manoj Kumar, M., Venkataramana, P., Yadagiri Swamy, P., and Chityala, Y. *N*-Amino-1,8-naphthalimide is a regenerated protecting group for selective synthesis of mono-*N*-substituted hydrazines and hydrazides. *Chemistry–A European Journal*, 27(70):17713-17721, 2021.

[33] Joshi, S. D., Dixit, S. R., Kulkarni, V. H., Lherbet, C., Nadagouda, M. N., and Aminabhavi, T.M. Synthesis, biological evaluation and in silico molecular modeling of pyrrolyl benzohydrazide derivatives as enoyl ACP reductase inhibitors. *European Journal of Medicinal Chemistry*, 126:286-297, 2017.

[34] Kumar, P., Narasimhan, B., Ramasamy, K., Mani, V., Mishra, R. K., and Majeed, A. B. A. Synthesis, antimicrobial, anticancer evaluation and QSAR studies of 2/3-bromo-*N*′-(substituted benzylidene/3-phenylallylidene) benzohydrazides. *Arabian Journal of Chemistry*, 10:S3740-S3748, 2017.

[35] Shundalau, M. B., Al-Abdullah, E. S., Shabunya-Klyachkovskaya, E. V., Hlinisty, A. V., Al-Deeb, O. A., El-Emam, A. A., and Gaponenko, S. V. Raman, infrared and DFT studies of N′-(adamantan-2-ylidene) benzohydrazide, a potential antibacterial agent. *Journal of Molecular Structure*, 1115:258-266, 2016.

[36] Arjun, H. A., Rajan, R. K., Elancheran, R., Ramanathan, M., Bhattacharjee, A., and Kabilan, S. Crystal structure, Hirshfeld surface analysis, DFT and molecular

docking studies on benzohydrazide derivatives as potential inhibitors of prostate cancer. *Chemical Data Collections*, 26:100350, 2020.

[37] Ohira, M., Iwasaki, Y., Tanaka, C., Kuroki, M., Matsuo, N., Kitamura, T., Yukuhiro, M., Morimoto, H., Pang, N., Liu, B., and Kiyono, T. A novel anti-microtubule agent with carbazole and benzohydrazide structures suppresses tumor cell growth *in vivo*. *Biochimica et Biophysica Acta (BBA)-General Subjects*, 1850(9):1676-1684, 2015.

[38] Melnyk, P., Leroux, V., Sergheraert, C., and Grellier, P. Design, synthesis and in vitro antimalarial activity of an acylhydrazone library. *Bioorganic & Medicinal Chemistry Letters*, 16(1):31-35, 2006.

[39] Becerra-Figueroa, L., Ojeda-Porras, A., and Gamba-Sanchez, D. Transamidation of carboxamides catalyzed by Fe(III) and water. *The Journal of Organic Chemistry*, 79(10):4544-4552, 2014.

[40] Nammalwar, B., Muddala, N. P., Watts, F. M., and Bunce, R. A. Efficient conversion of acids and esters to amides and transamidation of primary amides using OSU-6. *Tetrahedron*, 71(48):9101-9111, 2015.

[41] Rao, S. N., Mohan, D. C., and Adimurthy, S. Chitosan: an efficient recyclable catalyst for transamidation of carboxamides with amines under neat conditions. *Green Chemistry*, 16(9):4122-4126, 2014.

[42] Gomes, R., Bhanja, P., and Bhaumik, A. A triazine-based covalent organic polymer for efficient $CO_2$ adsorption. *Chemical Communications*, 51(49):10050-10053, 2015.

[43] Anfar, Z., Ait Ahsaine, H., Zbair, M., Amedlous, A., Ait El Fakir, A., Jada, A., and El Alem, N. Recent trends on numerical investigations of response surface methodology for pollutants adsorption onto activated carbon materials: a review. *Critical Reviews in Environmental Science and Technology*, 50(10):1043-1084, 2020.

[44] Allen, C. L., Atkinson, B. N., and Williams, J. M. Transamidation of primary amides with amines using hydroxylamine hydrochloride as an inorganic catalyst. *Angewandte Chemie International Edition*, 51(6):1383-1386, 2012.

[45] Frisch, M. J., Trucks, G. W., Schlegel, H. B., Scuseria, G. E., Robb, M., Cheeseman, J. R., Scalmani, G., Barone, V., Mennucci, B., Petersson, G. A., and Nakatsuji, H. Gaussian 09, revision D.01; Gaussian Inc., Wallingford CT, 2009.

## 2.6 Representative Spectra

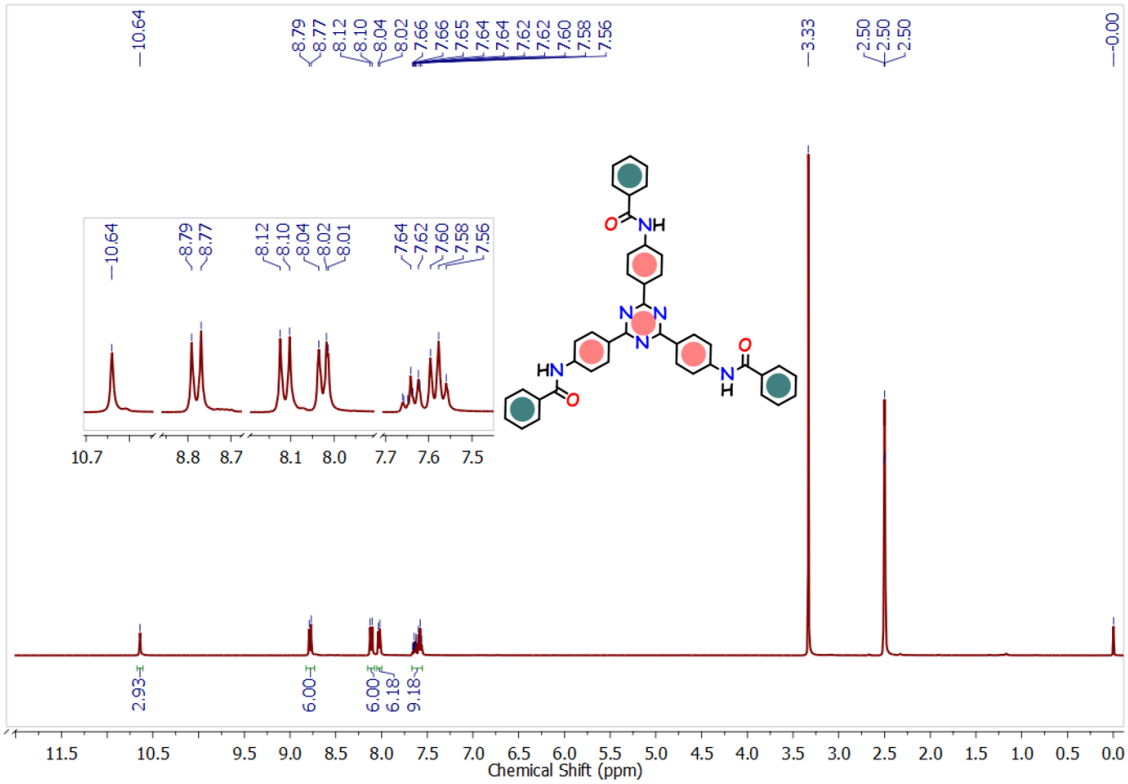


**Figure 2.10** $^{1}$H NMR (DMSO-d$_6$, 400 MHz, 298 K) of MOP-Am2-m

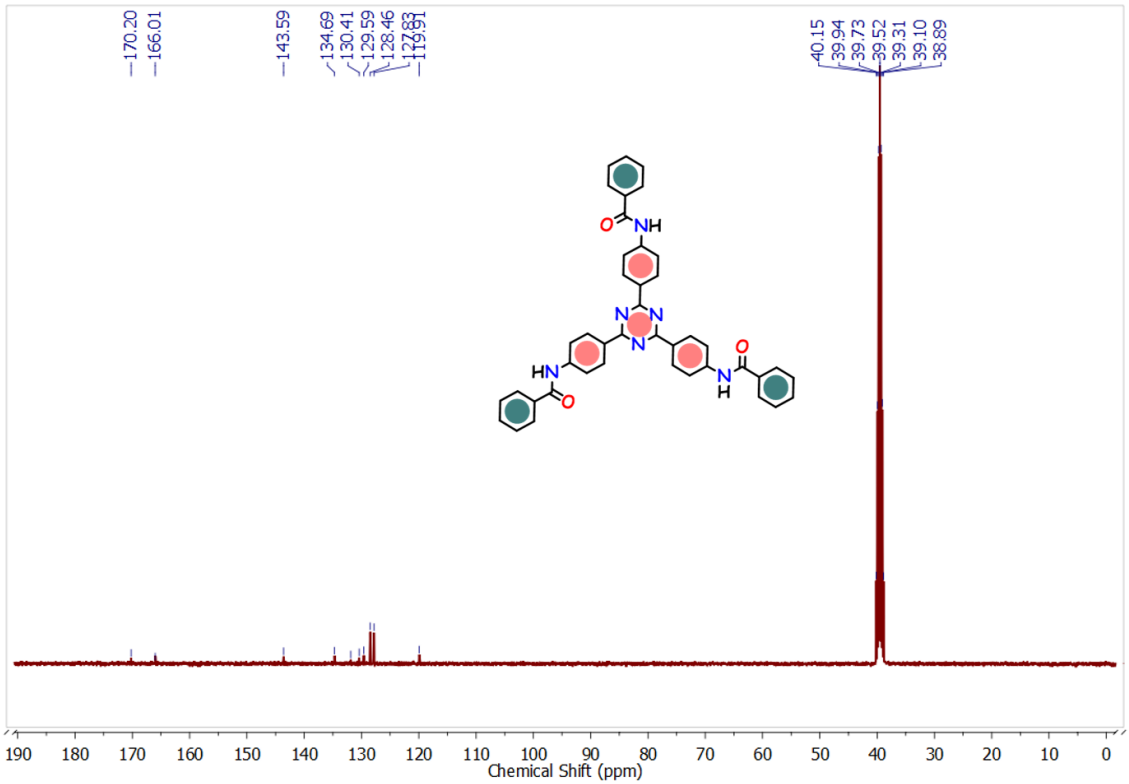


**Figure 2.11** $^{13}$C{$^{1}$H} NMR (DMSO-d$_6$, 101 MHz, 298 K) of MOP-Am2-m

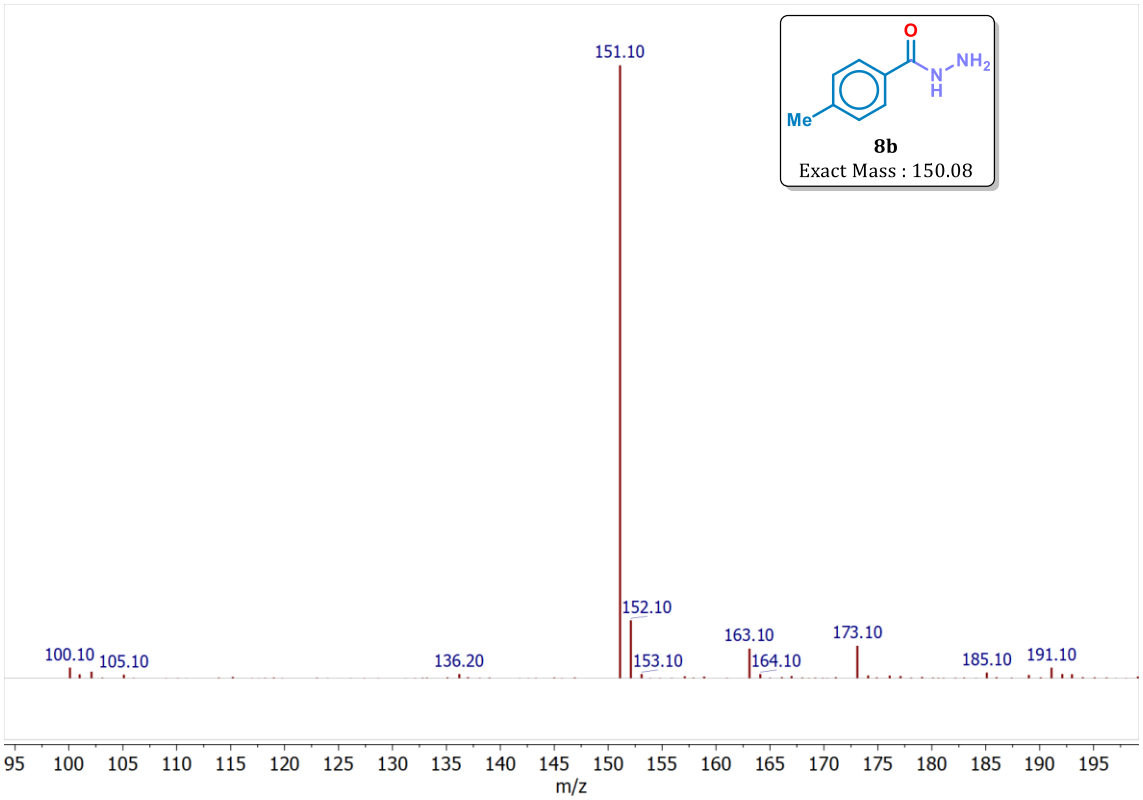


**Figure 2.12** LRMS (ESI⁺) *m/z* of **8b**

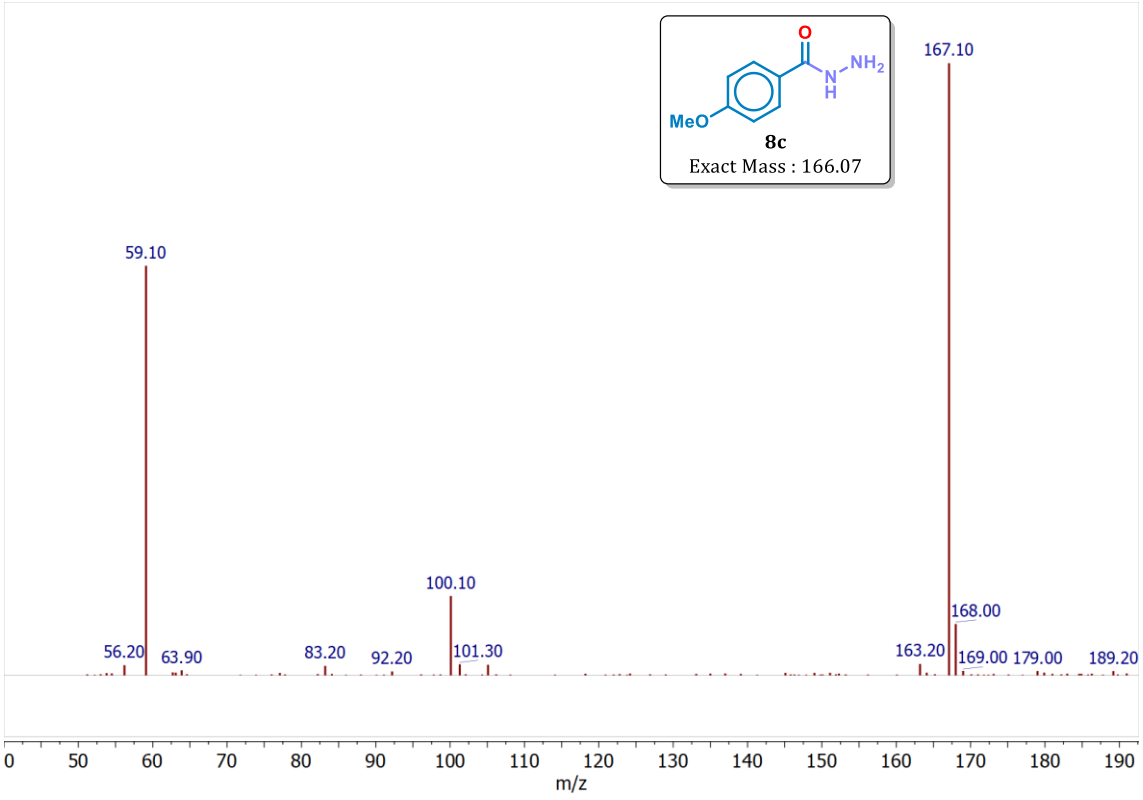


**Figure 2.13** LRMS (ESI⁺) *m/z* of **8c**

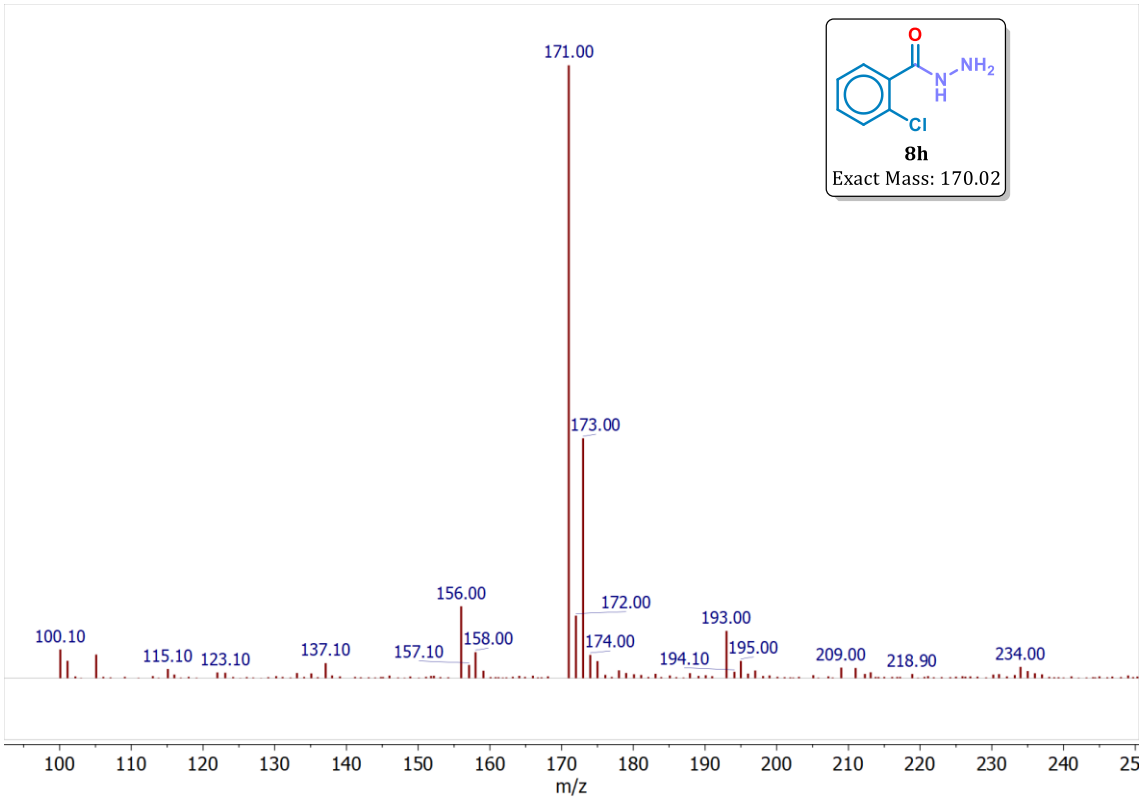


**Figure 2.14** LRMS (ESI⁺) *m/z* of **8h**

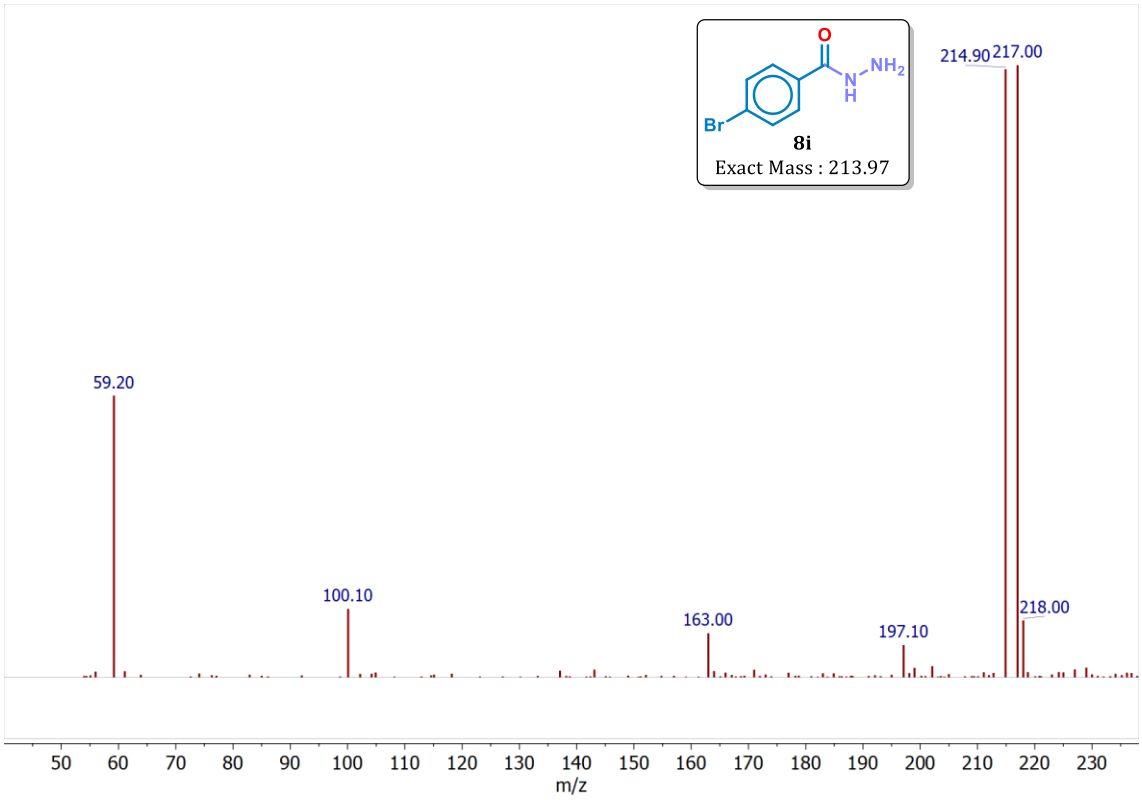


**Figure 2.15** LRMS (ESI⁺) *m/z* of **8i**